ChemComm

Accepted Manuscript

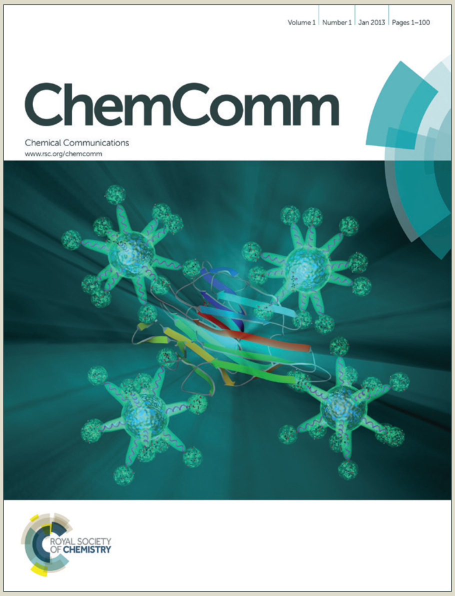

ROYAL SOCIETY OF CHEMISTRY

www.rsc.org/chemcomm

Chemical Communications

RSCPublishing

COMMUNICATION

Cite this: DOI: 10.1039/x0xx00000x

Building Ni_3S_2 nanotubes array and application as an electrode in lithium ion battery

Dan Li, Xiuwan Li, Xiaoyi Hou, Xiaolei Sun, Boli Liu and Deyan He*

Received 00th January 2012,
Accepted 00th January 2012

DOI: 10.1039/x0xx00000x

www.rsc.org/

Ni_3S_2 nanotubes array has been synthesized on Ni foam by a template-free hydrothermal method. The Ni foam acts as both reactant and support. Benefitting from the unique morphology, the resultant architectures as electrodes of lithium ion batteries exhibit excellent electrochemical performance with high capacity, long cycle life and superior rate capability.

With the increase consumption of fossil fuels and the aggravation of the global environmental pollution, there is an urgent need for finding alternative clean renewable energy. The high-performance energy storage devices become even more important for storing the renewable energy. Lithium ion batteries (LIBs) have gained more and more attention due to their high energy density, environment benignity, and reusable. However, the application of LIBs is limited mainly owing to the low capacities of the cathode materials, which inspired the researchers to search for better alternative cathode materials.[1-6] Ni_3S_2 as a promising candidate is of many advantages including higher theoretical capacity (472 mA h g^{-1}), innocuity, naturally abundant and low cost, and it is more suitable for largescale application in high-power devices.[7-9] In despite of so many attractive merits, the practical application of Ni_3S_2 as cathode of LIBs is still hampered by its low conductivity and poor capacity retention over extended cycling.[9, 10]

Strategies to overcome the mentioned drawbacks can be summarized into two common categories. One is to design various nanostructures, such as nanosheets, nanowires, and nanorods, because the nanostructured electrodes can alleviate the strain caused by repeated Li^+ insertion and extraction and avoid the possible rapid capacity fading.[11-13] Among various nanostructures, nanotubes stand out due to their one-dimensional (1D) structure facilitating electron and ion transport, their tubular geometry providing enough interior free space to accommodate the large volume change, and their large surface area making the electrodes and the electrolyte contact more fully. Template-assisted synthesis is one of the most widely used methods to prepare nanotubes. However, it often requires a rather tedious post-processing in order to remove the used template, making the approach to be costly, wasteful, and of environmental concern. Clearly, the problems can be solved if the nanotube structure could be achieved in a one-step template-free method. The another approach is to grow electroactive nanostructures on conductive substrates to form electrodes without additive. Compared with the traditional electrode preparation, the method can avoid the undesirable interface and inactive weight, and provides a better physical adhesion and electrical contact between the active material and current collector. However, a direct growth of free-standing and well-assembled Ni_3S_2 nanotubes array on current-collecting substrate has not been reported so far.

In this work, we have synthetized Ni_3S_2 nanotubes array on Ni foam for the first time by a facile and environmentally benign template-free hydrothermal route. The novel architecture integrates all the key features of a high-performance cathode of LIB. The specific capacity was 762 mA h g^{-1} in the 100th discharge/charge cycle at a current density of 100 mA g^{-1}. As the current density increased to 1000 mAh g^{-1}, it still delivered a capacity as high as 419 mA h g^{-1}. To the best of our knowledge, this is the best performance of Ni_3S_2 as cathode material of LIB, indicating that the material can be a promising candidate for LIB with high-power capability.

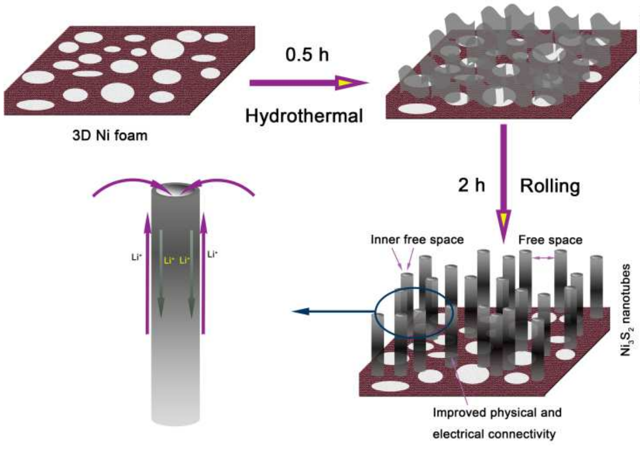

Scheme 1 Schematic illustration showing the synthesis of the Ni_3S_2nanotubes array on Ni foam and schematic diagram of Li^+ movement in a nanotube.

Based on the scanning electron microscopy (SEM) images observed for different reaction times shown in Fig. S1 (ESI†), the possible growth mechanism of the Ni_3S_2 nanotubes array in hydrothermal synthesis is proposed and shown in Scheme 1. Ni_3S_2 nanosheets are first obtained through the sulfuration of Ni foam. With the reaction proceeding, the area of the sheets and the number of the unsaturated dangling bonds on the surface increase. As a result, the surface activity of the sheets increases and the system energy is enhanced. The nanosheets curl into tubular morphology in order to reduce the system energy.[14] It should be pointed out that, at this stage, the exact mechanism behind the growth of the Ni_3S_2 nanotubes array is inconclusive and the further experiments are underway.

The possible chemical reactions are as follows:[15, 17]

$$S_2O_3^{2-} + H_2O \rightarrow SO_4^{2-} + H_2S \qquad (1)$$

$$H_2S + 2H_2O \rightarrow 2H_3O+ + S^{2-} \qquad (2)$$

$$2S^{2-} + O_2 + 2H_2O + 3Ni \rightarrow Ni_3S_2 + 4OH^- \qquad (3)$$

When the architecture of the synthesized Ni_3S_2 nanosheets array on Ni foam is used as a cathode of LIB, there are enough spaces between the nanotubes and inside the nanotubes, which not only accommodate the volume changes caused by the repeated lithiation and delithiation, but also facilitate lithium ions being transferred more effectively along the one-dimensional channel. Moreover, because the Ni_3S_2 nanotubes array was directly grown on the Ni foam, the better physical adhesion and electrical contact are obtained between the active material and the current collector.

Fig. S2 (ESI†) shows the X-ray diffraction (XRD) patterns of the as-synthesized Ni_3S_2 nanotubes array and the used Ni foam. As can be seen, the three strong diffraction peaks at 44.4°, 51.7°, and 76.2° appeare in the patterns, which correspond to (111), (200) and (220) faces of metallic nickel (JCPDS 04-0850), respectively. The other distinct diffraction peaks located at 21.7°, 31.1°, 37.7°, 38.2°, 50.1°, 55.1°, and 55.3° can be indexed to (010), (-110), (111), (-111), (-120), (-121) and (-211) planes of Ni_3S_2 (JCPDS 85-1802), respectively. No other peaks can be observed, suggesting the high purity of the sample.

Fig. 1a shows the low-magnification SEM image of a representative Ni_3S_2 nanotubes array. The cross-sectional SEM image of the sample is shown in the insert of Fig. 1a. It can be seen that the nanotubes are homogeneously aligned and intensively adhered to the Ni foam with an average thickness of about 1.75 μm. It is better to tolerate the volume change and improve the electrochemical performance when such an architecture is used as an electrode of LIBs. Fig. 1b shows a high-magnification SEM image of the Ni_3S_2 nanotubes array. The wall thickness of the nanotubes is very thin, and most of the nanotubes are rolled up by nanosheets. Fig. 1c and 1d show transmission electron microscopy (TEM) images of a nanotube exfoliated ultrasonically from the sample. It is confirmed that the diameter of the Ni_3S_2 nanotube is about 40 nm, and the wall thickness is estimated to be about 5 nm. The selected-area electron diffraction (SAED) pattern (insert of Fig. 1d) shows the well-defined diffraction rings, suggesting their polycrystalline structure. The measured lattice spacing of 0.287 nm shown in Fig. 1d is in good agreement with the (-110) interplanar distance of Ni_3S_2.

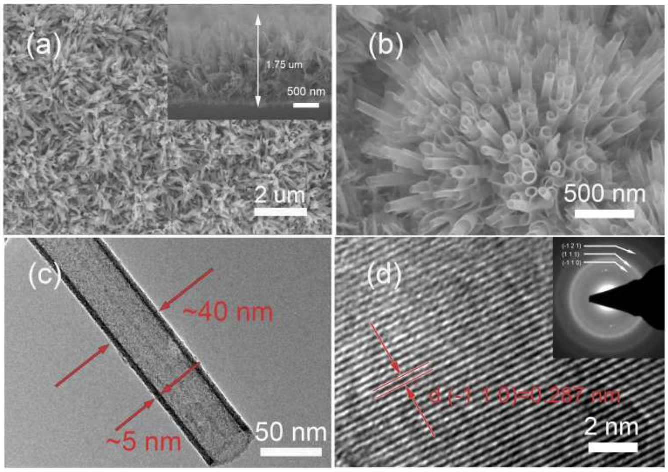

Fig. 1 (a) Low-magnification SEM image of a representative Ni_3S_2 nanotubes array synthesized on Ni foam for a reaction time of 2 h, and the insert is its cross-sectional morphology. (b) The high-magnification SEM image of the Ni_3S_2 nanotubes array. (c) TEM image of a single nanotube. (d) The high-resolution TEM image of the nanotube, and the insert is its SAED pattern.

The electrochemical performance of the as-synthesized Ni_3S_2 nanotubes array was evaluated by assembling the architecture into CR2032 coin cell as a cathode. Cyclic voltammetry (CV) curves recorded in a potential range of 0.02 – 3.0V (*vs*. Li^+/Li) at a scan rate of 0.1 mV s^{-1} are shown in Fig. 2a. In the first scan, three cathodic peaks at 0.75, 1.25, and 1.59 V are observed, which can be attributed to the insertion of Li^+ ($4Li^+ + 4e^- + Ni_3S_2 \rightarrow 3Ni + 2Li_2S$) and the formation of solid electrolyte interface (SEI) layer on the active material surface.[16] By contrast, there is a strong peak appeared around 1.4, 1.96, and 2.3 V in the reduction process due to the extraction of Li^+ ($3Ni + 2Li_2S \rightarrow Ni_3S_2 + 4Li^+ + 4e^-$). Obvious differences can be found between the first and the subsequent cycles. The reduction peak shifts to 1.35V and a new cathodic peak appears at 2.15 V in the second cycle owing to the activation of the material, which is similar to those reported in literatures. [11] The CV curves are well overlapped in the subsequent cycles, demonstrating the good reversibility of Ni_3S_2 nanotubes array electrode. The result was further confirmed by the discharge/charge profiles measurement. As shown in Fig. 2b, the discharge and charge plateaus match well with the corresponding reactions of the CV analysis. [17-20]

To obtain the evidence of high-power performance of the Ni_3S_2 nanotubes array electrode, the rate capability was investigated with current densities from 50 to 1000 mA g^{-1}. Fig. S4 (ESI†) shows the representative voltage profiles. The discharge potential decreases and the charge potential increases with increasing the discharge/charge rate, which can be ascribed to the kinetic effects of the material, leading to the higher over potential and lower capacity at higher current. As shown in Fig. 2c, the corresponding reversible capacities at 50, 100, 250, 500, and 1000 mA g^{-1} are 528, 495, 466, 453, and 418 mA h g^{-1}, respectively. It is noted that, although the capacities at higher currents fade rapidly, a satisfactory reversible capacity of 532 mA h g^{-1} is still restored after 160 cycles upon reducing the rate to 50 mA g^{-1}. Moreover, the initial coulombic efficiency of the Ni_3S_2 nanotubes array electrode is 83%, and it maintains at over 95% upon cycling, as shown in Fig. 2c.

Fig. 2d shows the cycling performance of the Ni_3S_2 nanotubes array electrode. The initial 22 cycles were carried out at a current density of 50 mA g^{-1}, then the current density was increased to 100 mA g^{-1} in the subsequent cycles. It can be seen that the capacity at 100 mA g^{-1} increases with cycling, and the discharge capacity increases to 766 mA h g^{-1} in the 100th cycle. Similar capacity increment phenomenon has been widely referred in transition metal oxide electrodes, and the most common explanation is that the decomposition of the electrolyte on the surface of the active materials leads to the reversible growth of the polymeric gel-like film.

The superior rate capability and reversibility capacity of the obtained Ni_3S_2 nanotubes array electrode could be ascribed to the following facts. (1) The enough void space within and between the nanotubes can buffer stresses caused by volume change during the discharge/charge processes and efficiently hold the structural integrity of the active material. (2) The nanotubes array of Ni_3S_2 with high surface-to-volume ratio and open place between nanotubes can ensure efficient electrolyte penetration and enhance the contact area between the active material and electrolyte. (3) 1D structure of the nanotubes can offer short diffusion path for lithium ions, and provide fast transport channels. (4) The self-supporting Ni_3S_2 morphology grown directly on Ni foam can improve the electrical contact between the active Ni_3S_2 and the current collector of Ni foam.

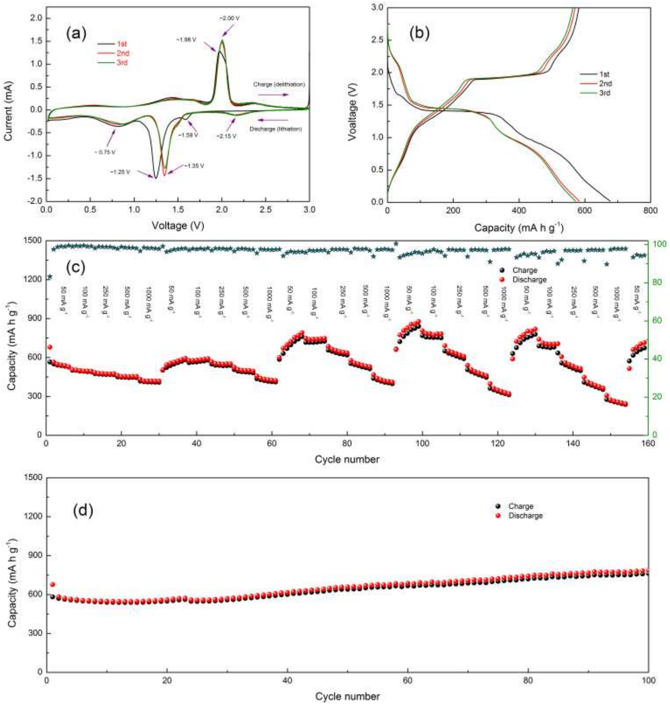

Fig. 2 Electrochemical performance of the Ni_3S_2 nanotubes array electrodes. (a) CV curves and (b) discharge/charge voltage profiles of the Ni_3S_2 nanotubes array electrode in the potential window of 0.02 – 3.0 V for the initial three cycles. (c) Rate performance of the Ni_3S_2 nanotubes array electrode with various current densities from 50 to 1000 mA g^{-1}. (d) Discharge/charge cyclings of the Ni_3S_2 nanotubes array electrode.

To further confirm the advantages of the self-supporting Ni_3S_2 electrode, electrochemical impedance spectroscopy (EIS) measurements were conducted after the electrodes being cycled for 3 and 30 times at 2.0 V *vs*. Li^+/Li with a current density of 500 mA g^{-1}. As shown in Fig. 3, the semicircle in the high-frequency region is assigned to the charge transfer resistance (R_{ct}). The small semicircle for the Ni_3S_2 nanotubes array electrode indicates its good conductivity, which can be ascribed to the open 1D structure, better adhesion and electrical contact as a result of the nanostructured Ni_3S_2 growing directly on Ni foam. The corresponding high-frequency portion of the Nyquist plots is shown in the insert of Fig. 3. The Ni_3S_2 nanotubes array electrode after 30 cycles corresponds to the high-frequency semicircle with the small diameter, indicating that there is smaller charge transfer resistance.[21]

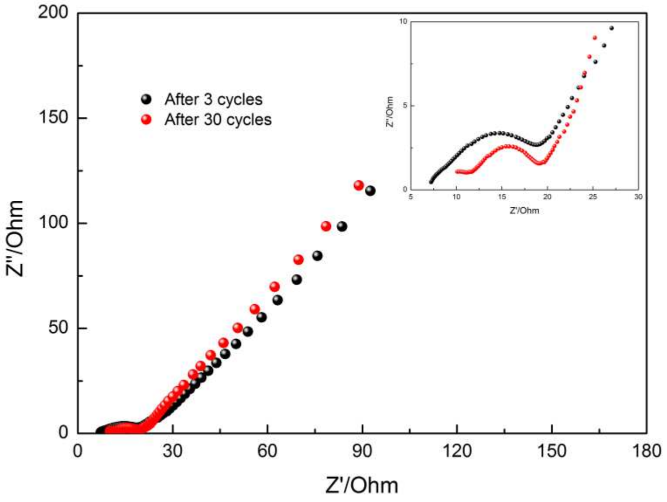

Fig. 3 Nyquist plots of the Ni_3S_2 nanotubes array electrode after 3 and 30 cycles respectively. The inset is the high-frequency portion.

Conclusions

In summary, novel Ni_3S_2 nanotubes array has been fabricated on Ni foam via a template-free hydrothermal method. As a cathode of LIBs, the unique architecture of the Ni_3S_2 nanotubes exhibits high capacity, excellent rate capability and cyclic stability. High reversible capacity of 533 mA h g^{-1} after 100 cycles at a rate of 100 mA g^{-1} and high capacity of 418 mA h g^{-1} at a rate as high as 1000 mA g^{-1} make the material a promising candidate for cathode material of high-power LIBs. Moreover, such a self-supporting Ni_3S_2 with nanotube morphology could find its interesting applications in other fields.

Notes and references

This project was financially supported by the National Natural Science Foundation of China with grant no. 11179038, and the Specialized Research Fund for the Doctoral Program of Higher Education with grant no. 20120211130005. D. Li gratefully acknowledges the support of the Fundamental Research Funds for the Central Universities with grant no. lzujbky-2014-234.

School of Physics Science and Technology, and Key Laboratory for Magnetism and Magnetic Materials of the Ministry of Education, Lanzhou University, Lanzhou 730000, China. Email: hedy@lzu.edu.cn (D. He); Tel.: +86 931 8912546; Fax: +86 931 8913554.

† Electronic Supplementary Information (ESI) available: Synthetic methods of Ni_3S_2 nanotubes array, SEM image of the used Ni foam substrate and the Ni_3S_2 nanostructures synthesized for different time, XRD and XPS of Ni_3S_2 nanotubes array, charge-discharge curves at various C rates and SEM images of the Ni_3S_2 nanotubes array electrode after cycles.

1 M. M. Thackeray, C. Wolverton and E. D. Isaacs, *Energy Environ. Sci.*, 2012, **5**, 7854.
2 R. Teki, M. K. Datta, R. Krishnan, T. C. Parker, T. M. Lu, P. N. Kumta and N. Koratkar, *Small*, 2009, **5**, 2236-2242.
3 Y. Li, Z.-Y. Fu and B.-L. Su, *Adv. Funct. Mater.*, 2012, **22**, 4634-4667.
4 Y.-S. Lee, J. H. Lee, J.-A. Choi, W. Y. Yoon and D.-W. Kim, *Adv. Funct. Mater.*, 2013, **23**, 1019-1027.
5 B. J. Landi, M. J. Ganter, C. D. Cress, R. A. Di Leo and R. P. Raffaelle, *Energy Environ. Sci.*, 2009, **2**, 638.

6 O. C. Compton, A. Abouimrane, Z. An, M. J. Palmeri, L. C. Brinson, K. Amine and S. T. Nguyen, *Small*, 2012, **8**, 1110-1116.
7 A. M. Cao, J. S. Hu, H. P. Liang and L. J. Wan, *Angew Chem Int Ed Engl*, 2005, **44**, 4391-4395.
8 S.-L. Chou, J.-Z. Wang, J.-Z. Sun, D. Wexler, M. Forsyth, H.-K. Liu, D. R. MacFarlane and S.-X. Dou, *Chem. Mater.*, 2008, **20**, 7044-7051.
9 M. R. Gao, Y. F. Xu, J. Jiang and S. H. Yu, *Chem. Soc. Rev.*, 2013, **42**, 2986-3017.
10 C.-H. Lai, M.-Y. Lu and L.-J. Chen, *J. Mater. Chem.*, 2012, **22**, 19.
11 C.-H. Lai, K.-W. Huang, J.-H. Cheng, C.-Y.Lee, W.-F. Lee, C.-T.Huang, B.-J. H wang and L.-J. Chen, *J. Mater. Chem.*, 2009, **19**, 7277.
12 L. Mi, Q. Ding, W. Chen, L. Zhao, H. Hou, C. Liu, C. Shen and Z. Zheng, *Dalton. Trans.*, 2013, **42**, 5724-5730.
13 L. Mi, Q. Ding, W. Chen, Z. Zheng, H. Hou, C. Liu and C. Shen, *RSC Advances*, 2012, **2**, 6817.
14 B. D. Yao, Y. F. Chan, X. Y. Zhang, W. F. Zhang, Z. Y. Yang and N. Wang, *Appl. Phys. Lett.*, 2003, **82**, 281.
15 Y. J. Yang and J. W. Xiang, *Applied Physics A*, 2005, **81**, 1351-1353.
16 L. Su, Z. Zhou and P. Shen, *The Journal of Physical Chemistry C*, 2012, **116**, 23974.
17 N. Feng, D. Hu, P. Wang, X. Sun, X. Li and D. He, *Phys. Chem. Chem. Phys.*, 2013, **15**, 9924-9930.
18 D. Li, X. Li, S. Wang, Y. Zheng, L. Qiao and D. He, *Acs Appl Mater Interfaces*, 2013, **6**, 648-654.
19 S. Ni, X. Yang and T. Li, *J. Mater. Chem.*, 2012, **22**, 2395.
20 X. Sun, X. Wang, L. Qiao, D. Hu, N. Feng, X. Li, Y. Liu and D. He, *Electrochim. Acta*, 2012, **66**, 204-209.
21 X. Li, D. Li, L. Qiao, X. Wang, X. Sun, P. Wang and D. He, *J. Mater. Chem.*, 2012, **22**, 9189.